THE JOURNAL OF PHYSICAL CHEMISTRY Letters

Subscriber access provided by UNIV OF NEWCASTLE

Letter

Temperature Induced Large Broadening and Blueshift in the Electronic Band Structure and Optical Absorption of Methylammonium Lead Iodide Perovskite

Jia-Yue Yang, and Ming Hu

J. Phys. Chem. Lett., **Just Accepted Manuscript** • DOI: 10.1021/acs.jpclett.7b01719 • Publication Date (Web): 28 Jul 2017

Downloaded from http://pubs.acs.org on July 29, 2017

Just Accepted

"Just Accepted" manuscripts have been peer-reviewed and accepted for publication. They are posted online prior to technical editing, formatting for publication and author proofing. The American Chemical Society provides "Just Accepted" as a free service to the research community to expedite the dissemination of scientific material as soon as possible after acceptance. "Just Accepted" manuscripts appear in full in PDF format accompanied by an HTML abstract. "Just Accepted" manuscripts have been fully peer reviewed, but should not be considered the official version of record. They are accessible to all readers and citable by the Digital Object Identifier (DOI®). "Just Accepted" is an optional service offered to authors. Therefore, the "Just Accepted" Web site may not include all articles that will be published in the journal. After a manuscript is technically edited and formatted, it will be removed from the "Just Accepted" Web site and published as an ASAP article. Note that technical editing may introduce minor changes to the manuscript text and/or graphics which could affect content, and all legal disclaimers and ethical guidelines that apply to the journal pertain. ACS cannot be held responsible for errors or consequences arising from the use of information contained in these "Just Accepted" manuscripts.

ACS Publications

The Journal of Physical Chemistry Letters is published by the American Chemical Society. 1155 Sixteenth Street N.W., Washington, DC 20036

Published by American Chemical Society. Copyright © American Chemical Society. However, no copyright claim is made to original U.S. Government works, or works produced by employees of any Commonwealth realm Crown government in the course of their duties.

Temperature Induced Large Broadening and Blueshift in the Electronic Band Structure and Optical Absorption of Methylammonium Lead Iodide Perovskite

Jia-Yue Yang[†] *and Ming Hu*[†‡,*]

[†]Institute of Mineral Engineering, Division of Material Science and Engineering, Faculty of Georesources and Materials Engineering, RWTH Aachen University, 52064 Aachen, Germany

[‡]Aachen Institute of Advanced Study in Computational Engineering Science (AICES), RWTH Aachen University, 52062 Aachen, Germany

ABSTRACT

The power conversion efficiency of hybrid halide perovskite solar cells is profoundly influenced by the operating temperature. Here we investigate the temperature influence on the electronic band structure and optical absorption of cubic $CH_3NH_3PbI_3$ from first-principles by accounting for both the electron-phonon interaction and thermal expansion. Within the framework of density functional perturbation theory, the electron-phonon coupling induces slightly enlarged band gap and strongly broadened electronic relaxation time as temperature increases. The large broadening effect is mainly due to the presence of cation organic atoms. Consequently, the temperature dependent absorption peak exhibits blueshift position, decreased amplitude and broadened width. This work uncovers the atomistic origin of temperature influence on the optical absorption of cubic $CH_3NH_3PbI_3$ and can provide guidance to design high-performance hybrid halide perovskite solar cells at different operating temperatures.

TOC Graphic

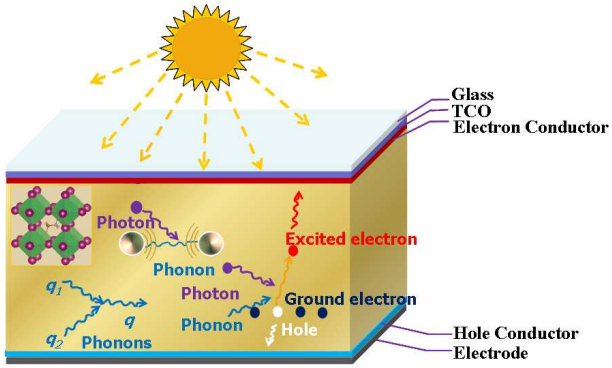

In span of few years, the energy conversion efficiency of organic-inorganic hybrid halide perovskites has enjoyed a remarkable increase from 3.8% in 2009 to 22.1% in 2016.[1-3] Besides, the hybrid halide perovskites, which mainly comprise earth-abundant elements and can be massively produced by simple solution-based processing techniques, have emerged as the most promising candidate for the next-generation high efficiency solar cell technology.[4-6] From materials point of view, they possess the perovskite-like structure and have the general formula of ABX_3, where A is a monovalent organic cation (typically methylammonium, $CH_3NH_3^+$), B is a divalent metallic atom (e.g. Pb, Ge or Sn), and X is a halogen atom (iodine, bromine or chlorine).[7, 8] In the crystal structure, the corner-shared BX_6^{4-} octahedral forms cubic or pseudo-cubic three-dimensional crystalline networks with the organic cations (A^+) filling the voids in the networks.

Ever since the first discovery of hybrid halide perovskites, numerous efforts have endeavored on the materials synthesis and processing, structural dynamics, charge-carrier transport, optical characterization and solar cell demonstration.[9-12] For the working device of thin film hybrid halide perovskite solar cell, its performance is intrinsically determined by the optical absorption and charge-carrier transport capabilities of the absorbers.[13-15] Thus, exploring the atomistic origin of optical absorption and charge transport in hybrid halide perovskites has become critical to advancing their applications in photovoltaics, in particular considering their structural instability and large sensitivity to temperature.[6, 16] The structural instability originates from the fact that the organic cation has lower symmetry than BX_6 octahedron and the neighboring organic molecules can align in different ways over various length scales. Due to the highly dynamic nature, the hybrid halide perovskites would experience phase transitions when the operating temperature varies between 162 K and 327 K.[17, 18] Consequently, the energy band alignment, absorption onset

and electronic dipole polarization will be disturbed. Foley and co-workers[19] reported a band gap increase of 30-40 meV in the methylammonium lead iodide for temperatures between 301 and 358 K via the ultraviolet photoemission spectroscopy and optical spectroscopy experiments. Saidi and co-workers[20] performed theoretical calculations by accounting for both the electron-phonon interaction and thermal expansion, and showed that the band gap increased by 40 meV within the temperature range of 290-380 K. The capacity to accurately determine temperature dependent energy levels has greatly motivated the computational design of novel perovskite solar cell absorbers. Yet it is of great necessity to explore the temperature dependence of optical absorption which is crucial to determining the energy conversion efficiency of hybrid halide perovskite solar cells under real conditions. However, the highly dynamic nature and the presence of heavy lead atoms make hybrid halide perovskite a challenging system to investigate from first-principles.[7, 21-24]

In this letter, we determine the temperature influence on electronic band structure and optical absorption of cubic $CH_3NH_3PbI_3$ perovskite from first-principles by accounting for both the electron-phonon coupling and thermal expansion. Prior to considering the electron-phonon coupling, the highly dynamic nature of the hybrid halide perovskite structure is demonstrated via analyzing the soft phonon modes in the phonon dispersion curves. Following the Allen-Heine-Cardona (AHC) theory,[25, 26] the temperature perturbed electronic band structure, such as edge shift and line broadening, can be captured by including up to the second-order term in the electron-phonon coupling. However, since the high-order terms in the electron-phonon coupling are neglected, the theoretically predicted band gap correction is overestimated and an energy scissor is introduced. Finally, with the temperature-perturbed electronic energy states, the

temperature-dependent optical absorption can be obtained following the electronic interband transition framework while including the excitonic (interacting electron-hole pair) effect.

Methodology. We perform first-principles calculations with the ABINIT[27, 28] software package. Those calculations were based on the optimized norm-conserving Vanderbilt pseudopotentials (ONCVPSP)[29] and the semilocal Perdew-Burke-Ernzerhof (PBE)[30] exchange-correlation functional. During the structural optimization and ground-state calculations, the force convergence threshold was set as 0.05 meV/Å. The electronic Brillouin zone was sampled using a 6×6×6 grid and the energy cutoff was 680 eV (see Supporting Information for convergence test). The relaxed lattice constant for the cubic $CH_3NH_3PbI_3$ perovskite is 6.32 Å, in good agreement with the value of 6.37 Å of ref 20. For the electron-phonon coupling calculations, the ***q***-point grid was chosen as 6×6×6, according to the convergence test from ref 20. The real part of the second-order electronic eigenvalues was calculated following AHC theory within the density functional perturbation theory (DFPT) framework,[31, 32] while the imaginary part related to electronic relaxation time was evaluated using the scheme of Fermi-Dirac smearing with the smearing width of 0.1 eV. To compute the optical absorption, the excitonic effect was included via solving the Bethe-Salpeter equation (BSE).[33, 34] Note that due to the computational limitation, the spin-orbit coupling was not considered in the present work.

Within the conventional density functional theory (DFT), atoms are assumed to be frozen at their crystallographic positions. However, the reality is that atoms vibrate even at absolute 0 K and lattice vibrations will induce the finite relaxation time of electrons and broadened absorption peak.[35-37] Based on the DFPT method, the lattice vibration is treated as an infinitesimal perturbation and its influence on electronic energy states is obtained within the scheme of

electron-phonon interaction.[38, 39] Following the AHC approach,[25, 26] the electronic energy state change due to the electron-phonon coupling at temperature T can be written as[40, 41]

$$\Delta E_{n\mathbf{k}}(T) = \int d\omega [N(\omega, T) + 1/2] \sum_{\nu} \frac{\partial E_{n\mathbf{k}}}{\partial N(\omega_{\upsilon}, T)} \delta(\omega - \omega_{\upsilon}), \quad (1)$$

where N is the Bose-Einstein statistics, E is the ground-state electronic energy and 1/2 corresponds to the zero-point vibration. The delta function δ ensures the energy conservation during electron-phonon interactions for all phonon modes υ. Then the finite temperature optical absorption can be obtained by solving BSE[33, 34] and given by[40]

$$\varepsilon_2(\omega) = -\frac{8\pi}{V} \sum_{n\mathbf{k}} \left| S_{n\mathbf{k}} \right|^2 \mathrm{Im}[(\omega - E^{FA}_{n\mathbf{k}} - \Delta E^{FA}_{n\mathbf{k}} + i\eta)^{-1}]. \quad (2)$$

The physical quantity S is the ground state electron-hole optical strength, η is a broadening parameter and V is the crystal volume.

Prior to performing electron-phonon coupling calculation, it is essential to peer into the dynamic nature of cubic $CH_3NH_3PbI_3$. In the phonon dispersion curves of Figure 1(a), we observe imaginary acoustic phonon modes centered around the high-symmetry R (q=1/2, 1/2, 1/2) and M (q=1/2, 1/2, 0) points. Those imaginary modes have been recently observed in the inelastic X-ray scattering (IXS) measurements[18, 42] and indicate its dynamical instability. Previous studies show that those soft phonon modes are due to the zone-boundary instabilities of perovskite structure and mainly associated with the collective titling of the corner-sharing BX_6^{4-} octahedral framework.[43, 44] Such interpretation is further verified by the projected density of states study which shows iodide atoms mainly contribute to the imaginary acoustic phonon modes, as shown in Figure 1(a). Although those soft phonon modes contribute to the strength of

electron-phonon coupling, yet their population is relatively small and the influence on electronic band structure and optical absorption is negligible.[20, 45] Furthermore, by analyzing the phonon dispersion relation, as shown in Figure 1(b)-(e), the phonon modes at high-symmetry points in the first Brillouin zone correspond to atomic motions, such as rotations and relative displacements, in the real space. Taking *M* point for instance, the normal vibrational modes are produced by the relative rotations of iodide atoms around lead atoms. In the meantime, the organic cations stretch and have relatively large freedom of motions, leading to the dynamic nature of hybrid halide perovskites.

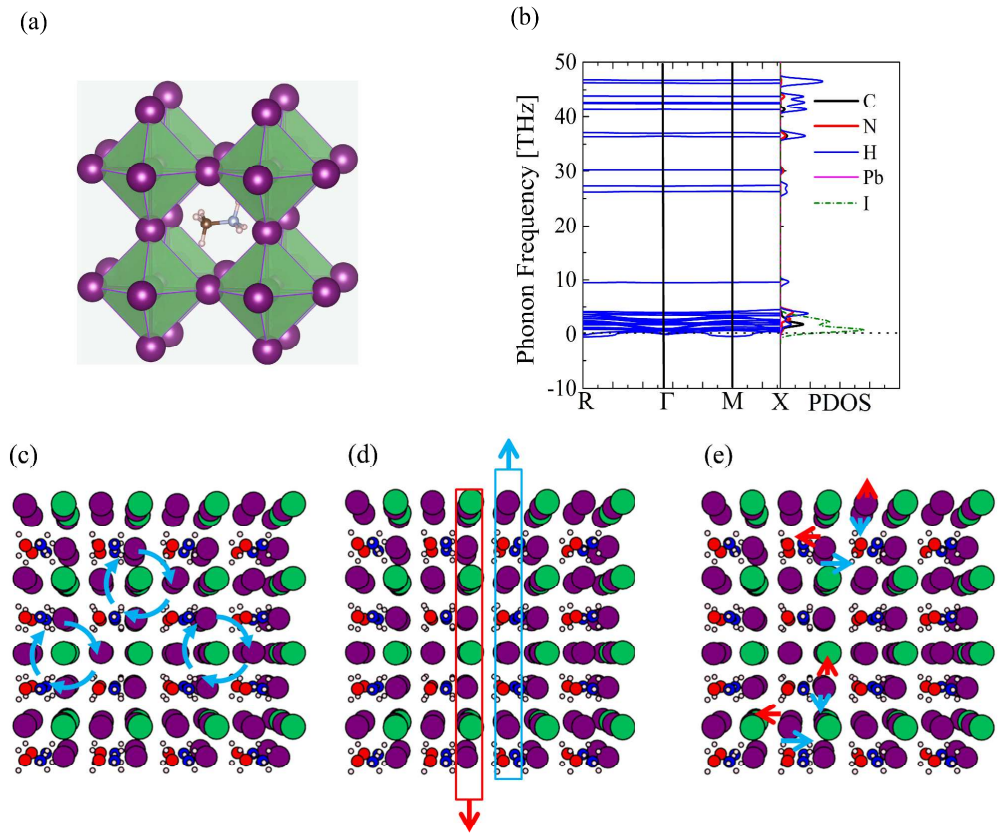

Figure 1. (a) Perovskite structure of cubic $CH_3NH_3PbI_3$, (b) the phonon dispersion curve and projected density of states (PDOS), and the corresponding atomic motions at high-symmetry points of (c) *M*, (d) *X* and (e) *R*. The arrows indicate the direction of atomic motions.

Due to its highly dynamic nature, the electron-phonon coupling in the cubic $CH_3NH_3PbI_3$ is relatively strong and it has been shown that the high-order terms make nontrivial contributions to the band gap correction even below 400 K.[20] However, the implemented AHC theory in this work can only include the electron-phonon coupling up to the second order term and the high-order terms are neglected.[25, 26] Thus, to reduce errors induced by the neglect of high-order terms, an energy scissor is introduced to correct the overestimated band gap. It makes sense because the focus of this work is on the temperature induced change in the electronic band structure, optical absorption and the atomistic origin for such change. Even though the high-order terms are not included in the theoretical calculations, it shows that the electron-phonon coupling demonstrates relatively large influence on the electronic band structure of cubic $CH_3NH_3PbI_3$. In Figure 2(a) and 2(b), it is observed that the electronic energy states in the low valence bands between -8 eV and -3 eV are greatly broadened by lattice vibrations at 300 K and 600 K, respectively. After projecting the density of states into individual element, the organic carbon, nitrogen and hydrogen atoms mainly contribute to those energy states between -8 eV and -3 eV.[46] So it assumes that such large broadening effect is mainly due to the presence of those organic atoms. To verify this assumption, we compare the electronic band structure of cubic $CH_3NH_3PbI_3$ and inorganic cubic $CsPbI_3$ at 600 K, as shown in Figure 2(b) and 2(c). By comparison, it is observed that there is no such strong line broadening for the inorganic $CsPbI_3$, which further justifies that the organic cation atoms mainly contribute to the strong electron-phonon coupling in the cubic $CH_3NH_3PbI_3$. Moreover, by analyzing the temperature-dependent band edges in details, we find a slight increase in the band gap as temperature increases. For the high-temperature cubic phase, a direct bandgap of 1.4 eV occurs at the *R* point of the cubic Brillouin zone at 0 K. As temperature increases from 300 K to 400 K, the band gap is enlarged by 86 meV, with the lowest

conduction band edge at *R* point decreasing by 30 meV and the highest valence band edge reducing by 116 meV. Upon considering the thermal expansion effect (see details in Supporting Information), the band gap is further widened by 60 meV, which coincides with previous first-principles simulations.[19, 47] However, the band gap change of 146 meV largely overestimates the experimental measurements of 30-40 meV,[19] which is mainly due to the neglect of high-order terms in the electron-phonon coupling.[20] On the other hand, due to the heavy Pb atoms involved, the spin-orbit coupling (SOC) can split the degenerate energy states in the conduction band and further lower the band gap correction.[20, 22, 23, 48-50] Thus, to correct the overestimated band gap change induced by the neglect of high-order terms and SOC effect, we apply an energy scissor during the optical absorption calculations of cubic $CH_3NH_3PbI_3$ over the temperature range of 200-500 K. The temperature-dependent band gap corrected by the energy scissor is provided in the Supporting Information.

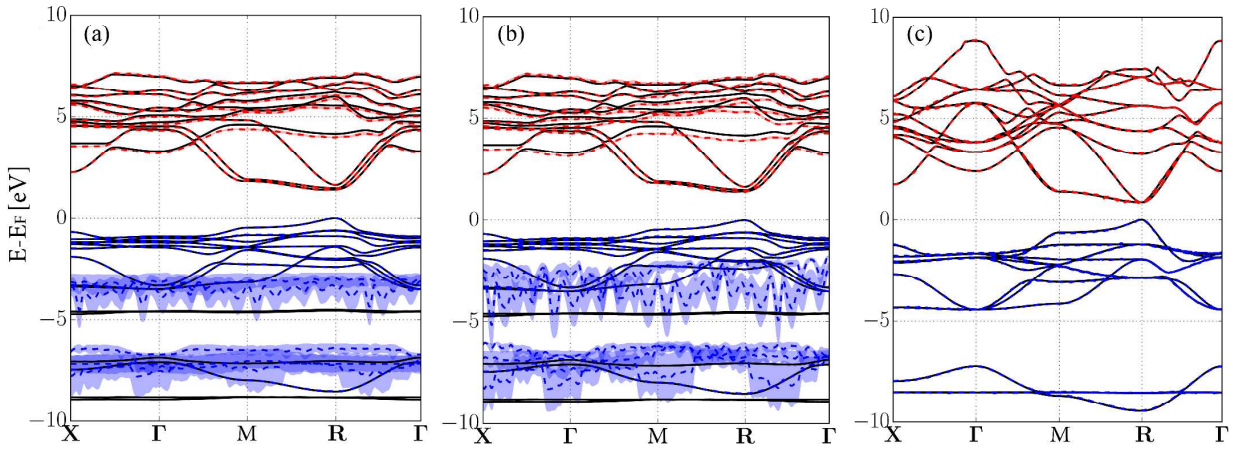

Figure 2. The electronic band structure of cubic $CH_3NH_3PbI_3$ at (a) 300 K, (b) 600 K, and (c) fully inorganic cubic $CsPbI_3$ at 600 K.

With the temperature-perturbed electronic band structure, it is feasible to obtain the optical absorption of cubic $CH_3NH_3PbI_3$ at finite temperature following the electronic interband

transition theory.[51, 52] Yet, prior to performing the temperature-dependent optical absorption calculations, it is essential to determine the many-body effect on optical properties, since it can not only correct the underestimated band gap by conventional DFT calculations[53] but also be crucial in accurately determining the optical transitions with the interacting electron-hole pair.[54] In Figure 3(a), we perform three different ground-state optical absorption calculations within the scheme of random phase approximation (RPA)[55], GW[56, 57] and BSE[33, 34], respectively, and compare those calculated results with literature experiment.[54, 58] The computational details about the optical absorption calculations are provided in the Supporting Information. With the GW approach, the band gap correction of 0.7 eV is applied for the ground state DFT computation. With the BSE method[33, 34], the excitonic effect is included into the electronic interband transition calculations. In comparison, it shows that the theoretically calculated optical absorption with the BSE method is in better agreement with experiments upon the inclusion of excitonic effect, as shown in Figure 3(a), indicating that the many-body effect is crucial to accurately determining the optical absorption peak. Thus, we include the excitonic effect into the optical absorption calculations of cubic $CH_3NH_3PbI_3$ and choose the temperature-perturbed electronic energy states as input to obtain the finite temperature optical absorption. Perturbed by lattice vibrations, the band gap is widened and line width is broadened at finite temperature and, thus, the electronic interband transition process is changed. In Figure 3(b), it is observed that the amplitude of absorption peak decreases, the position slightly shifts to higher energy and the width broadens as temperature increases. Such temperature effects on optical absorption are consistent with that in previous experiment[54] and can be interpreted by the temperature-perturbed electronic energy states. As lattice vibration is strengthened, the line broadening suggests that the electronic relaxation time is reduced and the population of electron energy states locating at the valence

band will decrease. Consequently, less electrons participate in the electronic interband transition and the optical transition strength is reduced, leading to the damped amplitude of the absorption peak. The blueshift of the absorption line can be explained by the widened band gap, and it requires higher photon energy to excite the ground state valence electrons to the conduction band. As for the broadened absorption peak, it is mainly caused by the decreased electronic relaxation time.

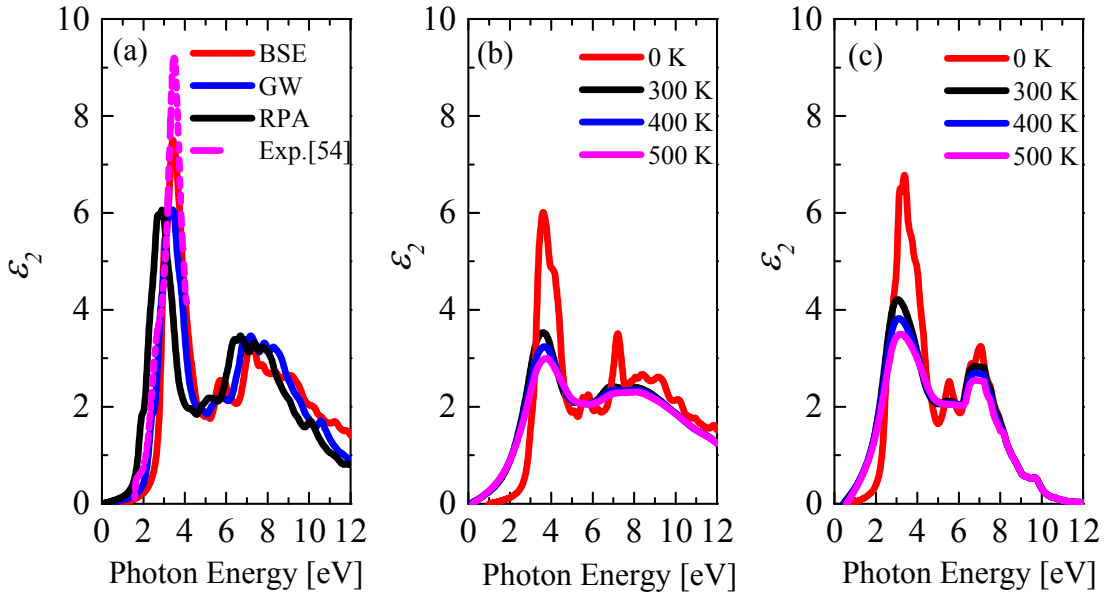

Figure 3. (a) The imaginary part of ground-state dielectric function of cubic $CH_3NH_3PbI_3$ calculated by the random phase approximation (RPA)[55], GW[56, 57] and BSE[33, 34], respectively, and compared with experiment[54]. The imaginary part of temperature-dependent dielectric function of (b) cubic $CH_3NH_3PbI_3$ and (c) inorganic $CsPbI_3$ calculated with the BSE theory by accounting for both the electron-phonon coupling and thermal expansion.

In contrast with the large broadening line in the electronic band structure due to the presence of organic cation atoms, the slightly broadened absorption peak of cubic $CH_3NH_3PbI_3$ suggests

that the organic cation atoms contribute little to the optical absorption. This can be interpreted from the view of electronic band structure that the organic cation atoms contribute less to the valence band maximum (VBM) and conduction band minimum (CBM).[46] On the other hand, we calculate the temperature-dependent optical absorption of inorganic $CsPbI_3$ as a comparison. In Figure 3(c), it shows that the dominant absorption peak of inorganic $CsPbI_3$ also demonstrates the slightly broadened width, blueshift position and decreased amplitude with increasing temperature, similar to that of cubic $CH_3NH_3PbI_3$. The similarity between the temperature-dependent optical absorption of inorganic $CsPbI_3$ and cubic $CH_3NH_3PbI_3$ further verifies that the inorganic Pb and I atoms mainly contribute to the optical absorption of hybrid halide perovskite at finite temperatures.

In summary, the temperature sensitivity of the electronic band structure and optical absorption of cubic $CH_3NH_3PbI_3$ is determined from atomic level using first-principles. Due to the collective tilting of octahedral framework, this hybrid halide perovskite demonstrates highly dynamical instability and there exist several soft phonon modes. Consequently, the electron-phonon coupling is relatively strong and electronic band structure is greatly perturbed by the lattice vibration, accompanied with the widened band gap and strong line broadening. Choosing those temperature-perturbed electronic energy states as input, the finite temperature optical absorption peak is modified with the decreased amplitude, blueshift position and broadened width. Moreover, the many-body effect is included via solving BSE and crucial in accurately determining the absorption peak. This work contributes to predicting the finite temperature optical properties of hybrid halide perovskites by accounting for electron-phonon coupling, thermal expansion and excitonic effect, which is not only relevant for the related solar cell

devices design but also can provide insight into the absorption and inverse radiative recombination processes.

AUTHOR INFORMATION

Corresponding Author

* E-Mail: hum@ghi.rwth-aachen.de (M.H.)

ORCID

Jia-Yue Yang: 0000-0002-3678-827X

Ming Hu: 0000-0002-8209-0139

Notes

The authors declare no competing financial interests.

ACKNOWLEDGMENTS

J.-Y. Yang gratefully acknowledges the computing time granted by the John von Neumann Institute for Computing (NIC) and provided on the supercomputer JURECA at Jülich Supercomputing Centre (JSC) (Project ID: JHPC37 and JHPC46). We greatly thank the Jülich Aachen Research Alliance-High Performance Computing (JARA-HPC) from RWTH Aachen University for granting us computing resources under Project No. jara0155.

ASSOCIATED CONTENT

Supporting Information

The Supporting Information is available free of charge on the ACS Publications website at DOI:.

Computational details on electron-phonon coupling with the AHC theory and optical absorption with the RPA, GW and BSE method, convergence test on plane-wave energy cutoff, thermal expansion effect and temperature-dependent band gap change for cubic $CH_3NH_3PbI_3$ as well as inorganic $CsPbI_3$.

REFERENCES

(1) Egger, D. A.; Rappe, A. M.; Kronik, L. Hybrid Organic–Inorganic Perovskites on the Move. *Acc. Chem. Res.* **2016,** *49*, 573-581.

(2) Jeon, N. J.; Noh, J. H.; Kim, Y. C.; Yang, W. S.; Ryu, S.; Seok, S. I. Solvent Engineering for High-Performance Inorganic–Organic Hybrid Perovskite Solar Cells. *Nat. Mater.* **2014,** *13*, 897-903.

(3) Sha, W. E. I.; Ren, X.; Chen, L.; Choy, W. C. H. The Efficiency Limit of $CH_3NH_3PbI_3$ Perovskite Solar Cells. *Appl. Phys. Lett.* **2015,** *106*, 221104.

(4) Gonzalez-Pedro, V.; Juarez-Perez, E. J.; Arsyad, W.-S.; Barea, E. M.; Fabregat-Santiago, F.; Mora-Sero, I.; Bisquert, J. General Working Principles of $CH_3NH_3PbX_3$ Perovskite Solar Cells. *Nano Lett.* **2014,** *14*, 888-893.

(5) Ball, J. M.; Lee, M. M.; Hey, A.; Snaith, H. J. Low-Temperature Processed Meso-Superstructured to Thin-Film Perovskite Solar Cells. *Energ. Environ. Sci.* **2013,** *6*, 1739-1743.

(6) Zhang, H.; Qiao, X.; Shen, Y.; Moehl, T.; Zakeeruddin, S. M.; Grätzel, M.; Wang, M. Photovoltaic Behaviour of Lead Methylammonium Triiodide Perovskite Solar Cells Down to 80 K. *J. Mater. Chem. A* **2015,** *3*, 11762-11767.

(7) Baikie, T.; Fang, Y.; Kadro, J. M.; Schreyer, M.; Wei, F.; Mhaisalkar, S. G.; Graetzel, M.; White, T. J. Synthesis and Crystal Chemistry of the Hybrid Perovskite $(CH_3NH_3)PbI_3$ for Solid-State Sensitised Solar Cell Applications. *J. Mater. Chem. A* **2013,** *1*, 5628-5641.

(8) Brenner, T. M.; Egger, D. A.; Kronik, L.; Hodes, G.; Cahen, D. Hybrid Organic—Inorganic Perovskites: Low-Cost Semiconductors with Intriguing Charge-Transport Properties. *Nat. Rev. Mater.* **2016,** *1*, 15007.

(9) Li, X.; Bi, D.; Yi, C.; Décoppet, J.-D.; Luo, J.; Zakeeruddin, S. M.; Hagfeldt, A.; Grätzel, M. A Vacuum Flash–Assisted Solution Process for High-Efficiency Large-Area Perovskite Solar Cells. *Science* **2016**, *353*, 58-62.

(10) Liu, M.; Johnston, M. B.; Snaith, H. J. Efficient Planar Heterojunction Perovskite Solar Cells by Vapour Deposition. *Nature* **2013,** *501*, 395-398.

(11) Frost, J. M.; Walsh, A. What Is Moving in Hybrid Halide Perovskite Solar Cells? *Acc. Chem. Res.* **2016,** *49*, 528-535.

(12) Hao, F.; Stoumpos, C. C.; Cao, D. H.; Chang, R. P. H.; Kanatzidis, M. G. Lead-Free Solid-State Organic-Inorganic Halide Perovskite Solar Cells. *Nat. Photon.* **2014,** *8*, 489-494.

(13) Frost, J. M.; Butler, K. T.; Brivio, F.; Hendon, C. H.; Van Schilfgaarde, M.; Walsh, A. Atomistic Origins of High-Performance in Hybrid Halide Perovskite Solar Cells. *Nano Lett.* **2014,** *14*, 2584-2590.

(14) Johnston, M. B.; Herz, L. M. Hybrid Perovskites for Photovoltaics: Charge-Carrier Recombination, Diffusion, and Radiative Efficiencies. *Acc. Chem. Res.* **2016,** *49*, 146-154.

(15) Eames, C.; Frost, J. M.; Barnes, P. R. F.; O/'Regan, B. C.; Walsh, A.; Islam, M. S. Ionic Transport in Hybrid Lead Iodide Perovskite Solar Cells. *Nat. Commun.* **2015,** *6,* 7497.

(16) Milot, R. L.; Eperon, G. E.; Snaith, H. J.; Johnston, M. B.; Herz, L. M. Temperature-Dependent Charge-Carrier Dynamics in $CH_3NH_3PbI_3$ Perovskite Thin Films. *Adv. Func. Mater.* **2015,** *25*, 6218-6227.

(17) Poglitsch, A.; Weber, D. Dynamic Disorder in Methylammoniumtrihalogenoplumbates (II) Observed by Millimeter-Wave Spectroscopy. *J. Chem. Phys.* **1987,** *87*, 6373-6378.

(18) Comin, R.; Crawford, M. K.; Said, A. H.; Herron, N.; Guise, W. E.; Wang, X.; Whitfield, P. S.; Jain, A.; Gong, X.; McGaughey, A. J. H.; et al. Lattice Dynamics and the Nature of Structural Transitions in Organolead Halide Perovskites. *Phys. Rev. B* **2016,** *94*, 094301.

(19) Foley, B. J.; Marlowe, D. L.; Sun, K.; Saidi, W. A.; Scudiero, L.; Gupta, M. C.; Choi, J. J. Temperature Dependent Energy Levels of Methylammonium Lead Iodide Perovskite. *Appl. Phys. Lett.* **2015,** *106*, 243904.

(20) Saidi, W. A.; Poncé, S.; Monserrat, B. Temperature Dependence of the Energy Levels of Methylammonium Lead Iodide Perovskite from First-Principles. *J. Phys. Chem. Lett.* **2016,** *7*, 5247-5252.

(21) Lindblad, R.; Bi, D.; Park, B.-w.; Oscarsson, J.; Gorgoi, M.; Siegbahn, H.; Odelius, M.; Johansson, E. M. J.; Rensmo, H. Electronic Structure of $TiO_2/CH_3NH_3PbI_3$ Perovskite Solar Cell Interfaces. *J. Phys. Chem. Lett.* **2014,** *5*, 648-653.

(22) Even, J.; Pedesseau, L.; Jancu, J.-M.; Katan, C. Importance of Spin–Orbit Coupling in Hybrid Organic/Inorganic Perovskites for Photovoltaic Applications. *J. Phys. Chem. Lett.* **2013,** *4*, 2999-3005.

(23) Filip, M. R.; Giustino, F. GW Quasiparticle Band Gap of the Hybrid Organic-Inorganic Perovskite $CH_3NH_3PbI_3$: Effect of Spin-Orbit Interaction, Semicore Electrons, and Self-Consistency. *Phys. Rev. B* **2014,** *90*, 245145.

(24) Brivio, F.; Butler, K. T.; Walsh, A.; van Schilfgaarde, M. Relativistic Quasiparticle Self-Consistent Electronic Structure of Hybrid Halide Perovskite Photovoltaic Absorbers. *Phys. Rev. B* **2014,** *89*, 155204.

(25) Allen, P. B.; Heine, V. Theory of the Temperature Dependence of Electronic Band Structures. *J. Phys. C: Solid State Phys.* **1976,** *9*, 2305.

(26) Allen, P. B.; Cardona, M. Theory of the Temperature Dependence of the Direct Gap of Germanium. *Phys. Rev. B* **1981,** *23*, 1495-1505.

(27) Gonze, X.; Jollet, F.; Abreu Araujo, F.; Adams, D.; Amadon, B.; Applencourt, T.; Audouze, C.; Beuken, J. M.; Bieder, J.; Bokhanchuk, A.; et al. Recent Developments in the ABINIT Software Package. *Comp. Phys. Commun.* **2016,** *205*, 106-131.

(28) Gonze, X.; Amadon, B.; Anglade, P.-M.; Beuken, J.-M.; Bottin, F.; Boulanger, P.; Bruneval, F.; Caliste, D.; Caracas, R.; Cote, M; et al. ABINIT: First-Principles Approach to Material and Nanosystem Properties. *Comp. Phys. Commun.* **2009,** *180*, 2582-2615.

(29) Schlipf, M.; Gygi, F. Optimization Algorithm for the Generation of ONCV Pseudopotentials. *Comp. Phys. Commun.* **2015,** *196*, 36-44.

(30) Perdew, J. P. Density-Functional Approximation for the Correlation Energy of the Inhomogeneous Electron Gas. *Phys. Rev. B* **1986,** *33*, 8822.

(31) Giannozzi, P.; Baroni, S. Density-Functional Perturbation Theory. In *Handbook of Materials Modeling: Methods*, Yip, S., Ed; Springer Netherlands: Dordrecht, 2005; *1*, 195-214.

(32) Gonze, X. Adiabatic Density-Functional Perturbation Theory. *Phys. Rev. A* **1995,** *52*, 1096-1114.

(33) Salpeter, E. E.; Bethe, H. A. A Relativistic Equation for Bound-State Problems. *Phys. Rev.* **1951,** *84*, 1232.

(34) Bickers, N. E.; Scalapino, D. J.; White, S. R. Conserving Approximations for Strongly Correlated Electron Systems: Bethe-Salpeter Equation and Dynamics for the Two-Dimensional Hubbard Model. *Phys. Rev. Lett.* **1989,** *62*, 961-964.

(35) Yang, J. Y.; Liu, L. H. Temperature-Dependent Dielectric Functions in Atomically Thin Graphene, Silicene, and Arsenene. *Appl. Phys. Lett.* **2015,** *107*, 091902.

(36) Yang, J. Y.; Liu, L. H.; Tan, J. Y. Temperature-Dependent Dielectric Function of Germanium in the UV–Vis Spectral Range: A First-Principles Study. *J. Quant. Spectrosc. Radiat. Transf.* **2014,** *141*, 24-30.

(37) Poncé, S.; Gillet, Y.; Laflamme Janssen, J.; Marini, A.; Verstraete, M.; Gonze, X. Temperature Dependence of the Electronic Structure of Semiconductors and Insulators. *J. Chem. Phys.* **2015,** *143*, 102813.

(38) Antonius, G.; Poncé, S.; Lantagne-Hurtubise, E.; Auclair, G.; Gonze, X.; Côté, M. Dynamical and Anharmonic Effects on the Electron-Phonon Coupling and the Zero-Point Renormalization of the Electronic Structure. *Phys. Rev. B* **2015,** *92*, 085137.

(39) Giustino, F. Electron-Phonon Interactions from First Principles. *Rev. Mod. Phys.* **2017,** *89*, 015003.

(40) Marini, A. Ab Initio Finite-Temperature Excitons. *Phys. Rev. Lett.* **2008,** *101*, 106405.

(41) Cardona, M. Electron–Phonon Interaction in Tetrahedral Semiconductors. *Solid State Commun.* **2005,** *133*, 3-18.

(42) Beecher, A. N.; Semonin, O. E.; Skelton, J. M.; Frost, J. M.; Terban, M. W.; Zhai, H.; Alatas, A.; Owen, J. S.; Walsh, A.; Billinge, S. J. L. Direct Observation of Dynamic Symmetry Breaking above Room Temperature in Methylammonium Lead Iodide Perovskite. *ACS Energ. Lett.* **2016,** *1*, 880-887.

(43) Marronnier, A.; Lee, H.; Geffroy, B.; Even, J.; Bonnassieux, Y.; Roma, G. Structural Instabilities Related to Highly Anharmonic Phonons in Halide Perovskites. *J. Phys. Chem. Lett.* **2017**, *8*, 2659-2665.

(44) Stokes, H. T.; Kisi, E. H.; Hatch, D. M.; Howard, C. J. Group-Theoretical Analysis of Octahedral Tilting in Ferroelectric Perovskites. *Acta Cryst. B* **2002,** *58*, 934-938.

(45) Whalley, L. D.; Skelton, J. M.; Frost, J. M.; Walsh, A. Phonon Anharmonicity, Lifetimes, and Thermal Transport in $CH_3NH_3PbI_3$ from Many-Body Perturbation Theory. *Phys. Rev. B* **2016,** *94*, 220301.

(46) Jong, U.-G.; Yu, C.-J.; Ri, J.-S.; Kim, N.-H.; Ri, G.-C. Influence of Halide Composition on the Structural, Electronic, and Optical Properties of Mixed $CH_3NH_3Pb(I_{1-x}Br_x)_3$ Perovskites Calculated Using the Virtual Crystal Approximation Method. *Phys. Rev. B* **2016,** *94*, 125139.

(47) Gonze, X.; Boulanger, P.; Côté, M. Theoretical Approaches to the Temperature and Zero-Point Motion Effects on the Electronic Band Structure. *Ann. Phys.* **2011,** *523*, 168-178.

(48) Amat, A.; Mosconi, E.; Ronca, E.; Quarti, C.; Umari, P.; Nazeeruddin, M. K.; Grätzel, M.; De Angelis, F. Cation-Induced Band-Gap Tuning in Organohalide Perovskites: Interplay of Spin–Orbit Coupling and Octahedra Tilting. *Nano Lett.* **2014,** *14*, 3608-3616.

(49) Menéndez-Proupin, E.; Palacios, P.; Wahnón, P.; Conesa, J. Self-Consistent Relativistic Band Structure of the $CH_3NH_3PbI_3$ Perovskite. *Phys. Rev. B* **2014,** *90*, 045207.

(50) Motta, C.; El-Mellouhi, F.; Kais, S.; Tabet, N.; Alharbi, F.; Sanvito, S. Revealing the Role of Organic Cations in Hybrid Halide Perovskite $CH_3NH_3PbI_3$. *Nat. Commun.* **2015,** *6*, 7026.

(51) Martin, R. M. *Electronic Structure: Basic Theory and Practical Methods*; Cambridge University Press: New York, USA, 2004.

(52) Peter, Y.; Cardona, M. *Fundamentals of Semiconductors: Physics and Materials Properties*; Springer-Verlag: Heidelberg, Germany, 2010.

(53) Antonius, G.; Poncé, S.; Boulanger, P.; Côté, M.; Gonze, X. Many-Body Effects on the Zero-Point Renormalization of the Band Structure. *Phys. Rev. Lett.* **2014,** *112*, 215501.

(54) Green, M. A.; Jiang, Y.; Soufiani, A. M.; Ho-Baillie, A. Optical Properties of Photovoltaic Organic–Inorganic Lead Halide Perovskites. *J. Phys. Chem. Lett.* **2015,** *6*, 4774-4785.

(55) Philipp, H.; Ehrenreich, H. Optical Properties of Semiconductors. *Phys. Rev.* **1963,** *129*, 1550.

(56) Rohlfing, M.; Louie, S. G. Excitonic Effects and the Optical Absorption Spectrum of Hydrogenated Si Clusters. *Phys. Rev. Lett.* **1998,** *80*, 3320.

(57) Albrecht, S.; Reining, L.; Del Sole, R.; Onida, G. Ab Initio Calculation of Excitonic Effects in the Optical Spectra of Semiconductors. *Phys. Rev. Lett.* **1998,** *80*, 4510.

(58) Xing, G.; Mathews, N.; Lim, S. S.; Yantara, N.; Liu, X.; Sabba, D.; Grätzel, M.; Mhaisalkar, S.; Sum, T. C. Low-Temperature Solution-Processed Wavelength-Tunable Perovskites for Lasing. *Nat. Mater.* **2014,** *13*, 476-480.

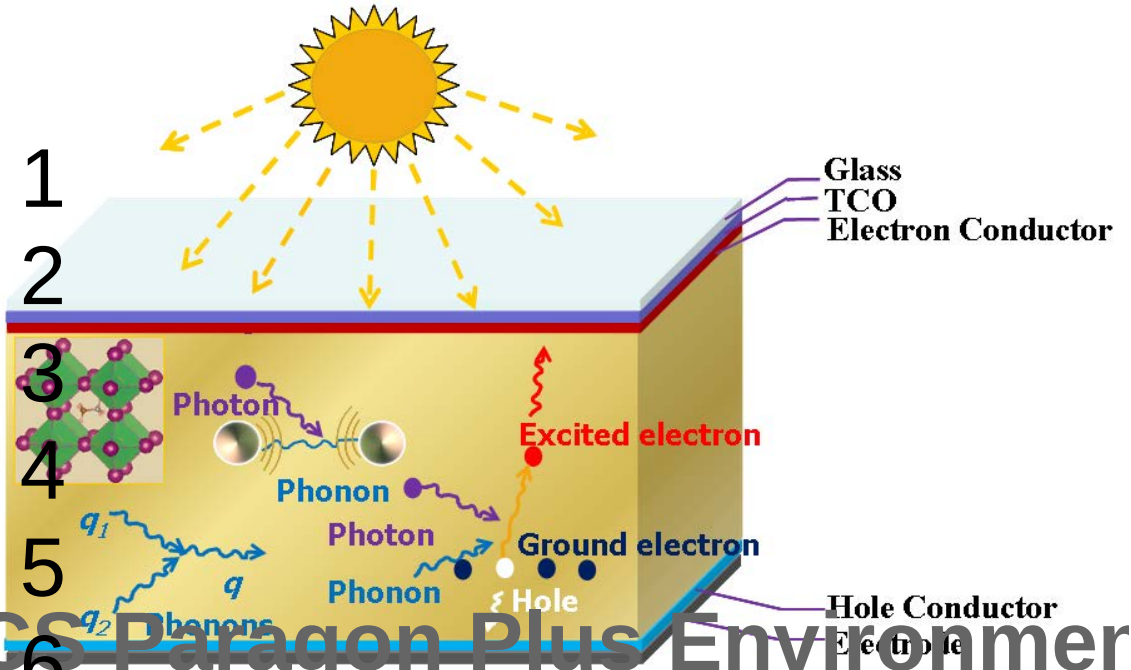

ACS Paragon Plus Environmen

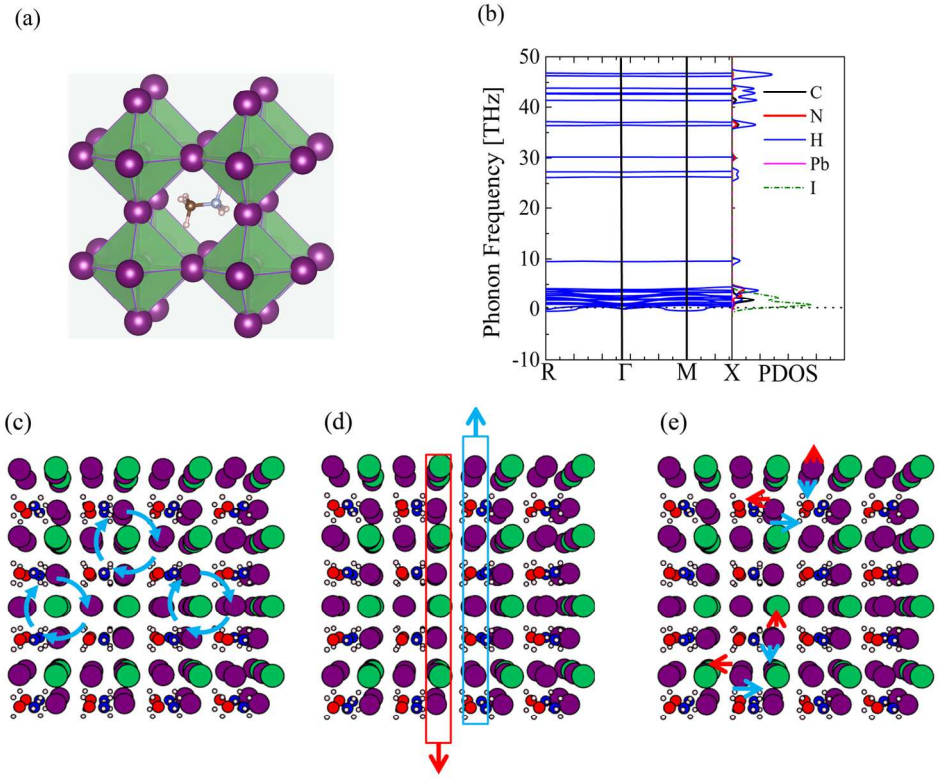

Figure 1. (a) Perovskite structure of cubic CH3NH3PbI3, (b) the phonon dispersion curve and projected density of states (PDOS), and the corresponding atomic motions at high-symmetry points of (c) M, (d) X and (e) R. The arrows indicate the direction of atomic motions.

149x124mm (300 x 300 DPI)

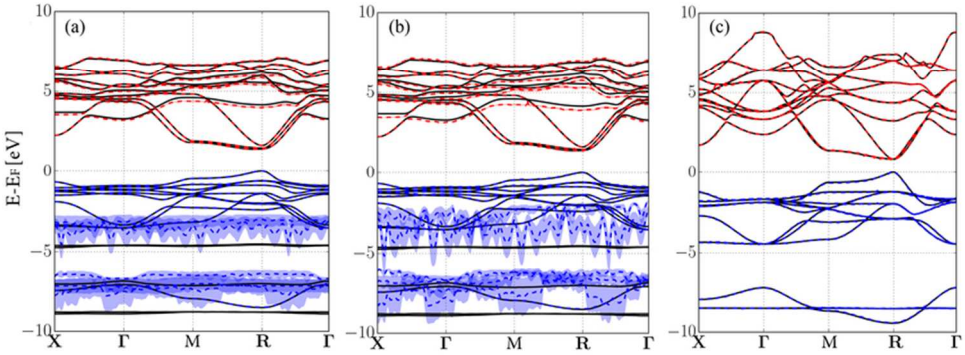

Figure 2. The electronic band structure of cubic CH3NH3PbI3 at (a) 300 K, (b) 600 K, and (c) fully inorganic cubic CsPbI3 at 600 K.

75x29mm (300 x 300 DPI)

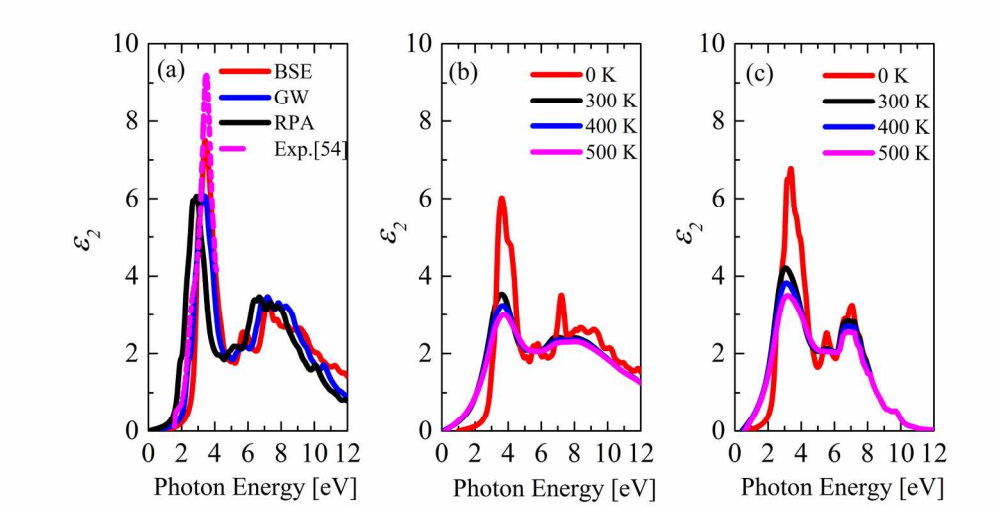

Figure 3. (a) The imaginary part of ground-state dielectric function of cubic CH3NH3PbI3 calculated by the random phase approximation (RPA)55, GW56, 57 and BSE33, 34, respectively, and compared with experiment54. The imaginary part of temperature-dependent dielectric function of (b) cubic CH3NH3PbI3 and (c) inorganic CsPbI3 calculated with the BSE theory by accounting for both the electron-phonon coupling and thermal expansion.

174x91mm (300 x 300 DPI)